Baghdad Science Journal

Volume 23 | Issue 4 Article 21

4-28-2026

Synthesis and Characterization of 1,3-thiazolidin-4-ones Using Recyclable, Magnetically Nanocatalyst in the Solvent-Free Microwave Medium

Jawad K. Abaies
Department of Chemistry, College of Science, University of Wasit, Wasit, Iraq, jabaies@uowasit.edu.iq

Athra G. Sager
Department of Chemistry, College of Science, University of Wasit, Wasit, Iraq, asaker@uowasit.edu.iq

Zeena R. Katoof
Department of Chemistry, College of Science, University of Wasit, Wasit, Iraq, zeenarazaq22@gmail.com

How to Cite this Article

Abaies, Jawad K.; Sager, Athra G.; and Katoof, Zeena R. (2026) "Synthesis and Characterization of 1,3-thiazolidin-4-ones Using Recyclable, Magnetically Nanocatalyst in the Solvent-Free Microwave Medium," *Baghdad Science Journal*: Vol. 23: Iss. 4, Article 21.
DOI: https://doi.org/10.21123/2411-7986.5274

BAGHDAD SCIENCE JOURNAL 2026;23(4):1425–1441

Scan the QR to view the full-text article on the journal website

RESEARCH ARTICLE

Synthesis and Characterization of 1,3-thiazolidin-4-ones Using Recyclable, Magnetically Nanocatalyst in the Solvent-Free Microwave Medium

Jawad K. Abaies, Athra G. Sager *, Zeena R. Katoof

Department of Chemistry, College of Science, University of Wasit, Wasit, Iraq

ABSTRACT

In the present work, an environmentally friendly nano-catalyst (γ Fe_2O_3RHA@SO_3H) was used for the preparation of 1,3-thiazolidin-4-ones analogs (T_1-T_9) from Schiff bases (S1-S9) by microwave irradiation. The recycled catalyst (γFe_2O_3RHA@SO_3H) was produced from silica derived from rice husk, which was first modified with ferrite nanoparticles (Fe_2O_3), then with sulfuric acid. The characterization of the (γ Fe_2O_3RHA@SO_3H)) nanocomposite and its characteristics were achieved using various techniques including, XRD, total acidity and basicity utilizing CO_2/NH_3-TPD, textural properties through Brunauer-Emmett-Teller (BET), functional group determination by FTIR; surface morphology through FESEM and TEM, magnetic properties by a vibrating sample magnetometer (VSM), and thermal stability via TGA. The VSM data demonstrated that the superparamagnetic catalyst (γFe_2O_3RHA@SO_3H) can be simply separated and recovered after reaction completion employing an external magnet. The attained data revealed that the optimum reaction parameters of the catalyst γFe_2O_3RHA@SO_3H for producing (S_1-S_9) were 5% (the catalyst amount), ethanol (the reaction solvent), 1h (the reaction time), and 70˚C (the reaction temperature) with a maximal yield up to 94%. The reusability study and reactivation results disclosed that the nano-bifunctional magnetic catalyst (γ Fe_2O_3RHA@SO_3H) can preserve a high catalytic activity after at least three reuses. The findings also indicated that (γ Fe_2O_3RHA@SO_3H) has superior magnetic characteristics, rendering it to be used as a heterogeneous catalyst in creation of 1,3-thiazolidin-4-one derivatives with high proficiency under simple reaction circumstances.

Keywords: Catalyst, Nanoparticle, Recycling, Schiff base, Silica

Introduction

Rice husk (RH) is an important source of silica as it is very cheap and available in abundance. Rice husk contains a high amount of amorphous silica. Exploiting this raw substance to extract silica is economically indispensable for the materials industry. Millions of tons of rice husk are burned yearly.[1,2] Burning rice husk produces rice husk ash (RHA).[3] Silica makes up about 95% of RHA, but burning rice husk causes environmental pollution. Instead, Hello and co-workers recently utilized a new approach to generate silica from rice husk.[4] They have successfully extracted silica from RH. They found that when burning RH in an oven, the amount of chemical pollutants launched into the air was notably minimized. Some of the hybrid organic-inorganic catalysts are produced by grafting silica (obtained from RH) with organic ligands. These catalysts have been effectively utilized in catalyzing various chemical reactions such as esterification,[5,6] acetalization of glycerol,[7] and cellulose hydrolysis.[8,9] In addition to the valuable role in catalyzing and supporting many organic reactions, the hybrid catalysts have been

Received 18 April 2025; revised 16 August 2025; accepted 5 September 2025.
Available online 28 April 2026

* Corresponding Author.
E-mail addresses: jabaies@uowasit.edu.iq (J. K. Abaies), asaker@uowasit.edu.iq (A. G. Sager), zeenarazaq22@gmail.com (Z. R. Katoof).

https://doi.org/10.21123/2411-7986.5274

successfully utilized in creating various nanoparticles. These nanoparticles have many potential applications due to their activity and stability in liquid media. As catalysts, utilizing nanoparticles (NPs) can enhance the catalytic activity and selectivity, and subsequently improve the catalyst system.[10] Because of the small size of nanoparticles (NPs) present in a catalyst system, the surface size will be expanded, resulting in the production of a semi-homogeneous media. Consequently, the gap between homogeneous and heterogeneous catalysts will be minimized.[11–14] The difficult separation and recovery of nanoparticles from the reaction medium is the main challenge in this approach. To overcome this issue, magnetic nanoparticle (MNPs) can be utilized as an alternative option. These MNPs can be isolated and acquired easily using an external magnet.[15] In this regard, superparamagnetic nanoparticles (MNPs) are considered superior supports for high-performance catalysts. Fe_3O_4 nanoparticles, in particular, are distinct catalyst supports as they are superparamagnetic, can be simply prepared, easily obtained, possess large surfaces, are cheap, and non-toxic.[16–18] The condensation reaction of a primary amine and an aldehyde produce Schiff bases accompanied by the loss of an H_2O molecule. In this reaction an acid molecule is commonly utilized as a catalyst. Due to the extensive applications of Schiff bases, they have drawn a lot of attention. These applications include HIV treatment[17–19] corrosion,[20] antibiotics, and fungus disease medications.[21] Also, Schiff bases are usually employed as ligands for metal coordination and catalysts.[22]

The Aims of the current study were to produce a magnetic heterogeneous nano-catalyst by immobilization of Fe_2O_3 onto silica (extracted from rice husk ash). The produced material was then immobilized using sulfuric acid to generate Bronsted sites. The formed heterogeneous nano-catalyst can be utilized in the preparation of Schiff bases. The separation of the stable nano-catalyst from the reaction vessel can be achieved using a simple magnetic bar. This catalyst can keep its activity in several reaction solvents, so it can be recycled over several sequential rounds retaining the catalytic activity.

Materials and methods

Materials and instrumental

Sodium hydroxide (99%), sulphuric acid (98%), ethanol (99.9%), aniline (99%), benzaldehyde (99%), vanillin (99%), bromobenzaldehyde (99%), chlorobenzaldehyde (99%), Ferric chloride ($FeCl_3$), and 4-aminoantipyrine (99%) were of AR grade, highly pure, and were utilized without additional purification. Rice husk (RH) was supplied by a rice mill factory in Wasit province, Iraq. Doubly distilled water was utilized in carrying out the reactions.

Powder X-ray diffraction (X' Pert Pro, monochromatized) was employed to acquire the XRD patterns in the range of 5°–90°. A transmission electron microscope (TEM) [(JEM-2100 (JEOL)] was utilized to investigate the surface morphological information of the synthesized γ $Fe_2O_3RH@SO_3H$. An energy dispersive spectrometer (EDX) was exploited to ascertain the surface elemental constitution of γ $Fe_2O_3RH@SO_3H$. A vibrating-sample magnetometer was used to test the sample magnetic characteristics at a magnetic field of 20 kOe. Melting points were measured in open capillary tubes; they were determined employing a Büchi B-545 apparatus. ^1H and ^{13}C NMR spectra were attained exploiting a 400 and 100 MHz Bruker Avance DRX spectrometers.

Source of silica

As abundant amounts of RH were available, it was utilized to produce amorphous silica. After extraction of silica from RHA, it was reacted with γ-Fe_2O_3.

Preparation of γFe_2O_3RHA

The solution (1): Amorphous silica (500mg) was dispersed in (50 mL) of distilled water with stirring for 1h. Solution 2: The nanoparticle Fe_2O_3 was prepared via a co-precipitation method of Fe(III) and Fe(II) ions in an alkali solution. $FeCl_2.4H_2O$ (0.01mol) and anhydrous $FeCl_3$(0.01) were dissolved in distilled water (25 mL) separately. The produced iron salt solutions were mixed with a robust stirring (500 rpm). To this mixture, a urea solution (0.02 mol, 50 mL) was added at room temperature. Solution (1) was then straightly added with continuous stirring. The produced mixture was then left stirring for 3h at ambient temperature. Meanwhile, sodium hydroxide (2N) was added dropwise. The product was left with a robust stirring for 1h at room temperature, then it was refluxed for 1h to produce a black dispersion material. Repeated centrifugation concentration was achieved to purify the produced magnetic nanoparticles. Upon collecting the materials, they were washed three times with ethanol. The obtained silica-coated nanoparticles were subjected to a vacuum for 24h for drying before being calcined for1h at 200°C.

Preparation of γ $Fe_2O_3RHA@SO_3H$

A solution of NaOH (1M) was added to $\gamma Fe_2O_3RHA@SO_3H$(2 gm) with stirring at room

temperature. To this mixture, (5%) H_2SO_4 was added dropwise. The produced material was filtered and washed before being dried at 100°C. Upon the modification process, the resulting catalyst was described as γ Fe_2O_3RHA@SO_3H.

Synthesis of Schiff base by using γ Fe_2O_3RHA@SO_3H Catalyst(S_1-S_9)

A mixture of amino compound (1mmol), aldehyde compound (1mmol), ethanol (10mL), and γ Fe_2O_3RHA@SO_3H (250 mg) was refluxed at 67°C for 2h with continuous stirring. The formed catalyst was isolated using an external magnet. After the unwanted products were filtered off, the obtained homogenous solution was cooled utilizing an ice bath. The mixture was then filtered to produce the desired Schiff bases. Investigation of the catalytic activity of the product materials was carried out following the procedure mentioned above under different conditions: various catalyst masses (500, 100, 150, and 200 mg), different temperatures[23] (room temperature 50, and 67°C), and different solvents (ethanol, 1-propanol, and DMF).

Selected spectroscopic data

N,1-diphenylmethanimine(S1):Orange precipitate; mp.=54°C; Rf=0.52: FT-IR cm^{-1}(KBr): 3112, 1612, 1591, 1481, 1396, 1408, 1093, 910, 813. ^{1}HNMR(400 MHz, DMSO-d6)δ: 8.39 (s, 1H, CH=N), 7.55(s,2H), 7.36(d, J=12.0Hz, 3H), 7.26(s,5H), 6.86(s,1H) (shown in Fig. S1). ^{13}CNMR(101MHz,DMSO-d6)δ: 166 (CH=N), 140 (C-N), 135-123 (aromatic carbons), 39 (DMSO, Solvent).[23]

1-(4-chlorophenyl)-N-phenylmethanimine(S_2): Yellow precipitate; mp.=252°C; R_f= 0.8; FT-IR cm^{-1} (KBr): 3422, 3080,2869, 1619, 1591, 1481, 1396, 1080,912,826,758. ^{1}HNMR (400 MHz, DMSO-d6) δ: 7.41 (s, 1H, CH=N), 6.77 (d, J = 14.9 Hz, 2H, Ar-H), 6.38 (t, J = 17.7 Hz, 2H, Ar-H), 6.26 (t, J = 11.4 Hz, 4H, Ar-H), 5.99 – 5.12 (m, 1H, Ar-H) (shown in Fig. S2).. ^{13}C NMR (101MHz, DMSO-d6)δ:167(CH=N),153(C-N),142-123.8 (aromatic carbons), 39 (DMSO) (shown in Fig. S3).

1-(4-bromophenyl)-N-phenylmethanimine(S_3): Brown precipitate; mp.=75°C; R 0.80; FT-IR cm^{-1}(KBr): 3110,2871,1650,1620, 1563, 1484, 1399, 1020. ^{1}H NMR (400 MHz, DMSO-d6) δ: 7.80 (s, 1H, CH=N), 7.12 (d, J = 8.3 Hz, 2H,Ar-H), 6.76 (d, J = 8.3 Hz, 2H, Ar-H), 6.58 (t, J = 7.6 Hz, 2H), 6.42 (t, J = 7.8 Hz, 3H) (shown in Fig. S4). ^{13}C NMR (101 MHz, DMSO-d6) δ: 159.5(CH=N), 152(aromatic carbon), 136 (C-N), 135-121 (aromatic carbons),39 (DMSO) (shown in Fig. S5).

3-methoxy-4-((phenylimino)methyl)phenol(S_4): Yellow precipitate; mp.=238°C; R_f=0.68; FT-IR cm^{-1}(KBr): 3461, 3092,2881,1662,1610, 1553, 1483. ^{1}HNMR (400 MHz, DMSO-d6)δ: 9.9 (s, 1H,OH), 8.8 (s, 1H,CH=N), 7.7 (d, J = 14.9 Hz, 1H, Ar-H), 7.5 (d, J = 7.0 Hz, 4H, Ar-H), 7.1 (d, J = 16.7 Hz, 1H, Ar-H), 6.5(t, J = 7.5 Hz, 2H, Ar-H), 3.8(s, 2H,CH_3) (shown in Fig. S6). ^{13}CNMR (101 MHz, DMSO-d6) δ: 166.1 (CH=N), 163.3 (C-OH), 162.9 (C-OCH_3), 149.3-100.1(aromatic carbons), 57(OCH_3), 39.5(DMSO).

4-(benzylideneamino)-1,5-dimethyl-2-phenyl-1,2-dihydro-3H-pyrazol-3-one(S_5): Pink precipitate; mp. =237°C; R_f =0.38; FT-IR cm^{-1}(KBr): 3743, 3082, 2930, 2872, 1651, 1629, 1568, 1480, 1366, 1127, 1110, 832; ^{1}HNMR (400 MHz, DMSO-d6) δ: 8.7(s, 1H,CH=N), 7.4(d, J= 72.0 Hz, 3H, Ar-H), 7.1 (d, J = 12.0 Hz, 4H,ArH), 6.8 (d, J=12.0 Hz, 4H,ArH), 2.3(s,3H,NCH_3),1.75 (s,3H,CH_3). ^{13}CNMR(101MHz, DMSO-d6)δ: 160(C=O), 148(CH_3-heterocyclic)137(C=N), 133-122(aromatic carbons),39(DMSO),33(N-CH_3),12 (CH_3).

4-((4-chlorobenzylidene)amino)-1,5-dimethyl-2-phenyl-1,2-dihydro-3H-pyrazol-3-one(S_6): Brown precipitate; mp.=245°C; R_f = 052; FT-IR cm^{-1} (KBr): 3741, 3110, 2930, 1649, 1630, 1570, 1485, 1376, 1132, 1083, 832, 765, 699; ^{1}HNMR (400 MHz, DMSO-d_6) δ: 8.70 (s, 1H,CN=N), 6.96 (s, 2H), 6.51 (t, J=57.6 Hz, 9H), 1.88 (s, 1H,CH_3), 1.23 (s, 2H,CH_3) (shown in Fig. S7). ^{13}CNMR(101MHz, DMSO-d6)δ: 161.00(C=O), 149.01(CH=N), 138.13(Heterocyclic), 135- 122 (aromatic carbons), 39 (DMSO), 33 (CH_3N), 11 (CH_3).

4-((4-bromobenzylidene)amino)-1,5-dimethyl-2-phenyl-1,2-dihydro-3H-pyrazol-3-one(S_7): Yellow precipitate; mp. =265°C; R_f = 0.67; FT-IR cm^{-1} (KBr): 3652, 3120, 1649, 1493,1396. ^{1}HNMR (400 MHz, DMSO-d6) δ: 9.5 (s, 1H,CH=N), 7.8 (s, 2H,Ar), 7.9–7.2(m, 9H,Ar), 3.2(s, 3H,CH_3), 2.3(s, 3H, CH_3). ^{13}CNMR (101 MHz, DMSO-d6)δ:171.5(C=O),159.5(C-N, Heterocyclic), 148 (C=N),143-134(aromatic carbons), 133 (C-Br),43(CH_3), 39 (solvent/ DMSO), 21 (CH_3).

4-((4-hydroxy-2-methylbenzylidene)amino)-1,5-dimethyl-2-phenyl-1,2-dihydro-3H-pyrazol-3-one(S_8): Orange precipitate; mp=237°C; Rf=0.57; FT-IR cm^{-1} (KBr): 3452, 3250, 3073, 2991, 2831, 1634, 1619, 1561, 1493, 1361, 1132,1087, 879. ^{1}HNMR (400 MHz, DMSO-d6)δ: 9.8(s,1H,OH),9.5 (s, 1H,CH=N), 7.61 (d, J = 8 Hz, 3H), 7.41 (d, *J* = 3 Hz, 3H), 6.80 (d, J = 6 Hz, 2H), 3.22 (s, 3H,CH_3), 2.5(DMSO), 2.42(s, 3H, CH_3),1.85(s, 3H, CH_3). ^{13}CNMR (101 MHz, DMSO-d6)δ:161(C=O),156

(C=OH),149 (Heterocyclic), 138.3(CH=N), 137 -110 (aromatic carbons), 39 (DMSO), 33 (CH_3), 18.0(CH_3), 11.0(CH_3).

N′-(4-hydroxy-3-methoxybenzylidene)isonicotinohydrazide(S_9). Yellow precipitate; mp.=238°C; FT-IR cm^{-1} (KBr): V (OH)3360-3530, 3240, 3028, 3001, 2941, 2829 (H alph.), 1595, 1550, 1510, υ(C-O) 1271, 10643, ^{1}HNMR (400 MHz, DMSO-d6)δ: 3.84 (3H, s, OCH3), 8.8-6.8 (7H, m, Ar-H), 8.36 (1H, s, CH=N), 9.7 (1H, s, OH), 11.9 (1H, s, NH-C=O). ^{13}CNMR (101 MHz, DMSO-d6)δ:161 (C=O), 150-109 (aromatic carbons), 148 (**C= N**), 56 (OCH_3).

Synthesis of 1,3-thiazolidin-4-ones by using γ Fe_2O_3RHA@SO_3H catalyst

γ Fe_2O_3RHA@SO_3H catalyst (0.05 mg), thioglycolic (5 mol), and Schiff base(S_1-S_8)(5 mmol) were mixed in a sealed round-bottomed flask and subjected to a microwave irradiation synthesizer with a maximum microwave power level of 400 W. The temperature of the reaction mixture was raised to 90°C. The reaction progress was monitored using TLC (hexane:ethanol 3:2). Upon completion of the reaction, the product was cooled and then neutralized using a 5% $NaHCO_3$ solution. The precipitate was separated by filtration, and then washed with distilled water five times. Finally, the solid product was recrystallized using an appropriate solvent.

Selected spectroscopic data

N,1-diphenylmethanimine(T_1): Brown precipitate; mp.=61°C: FT-IR cm^{-1}(KBr): 3080,3002, 1720, 1591, 1515., 1394, 1412, 1097,910, 813. ^{1}H NMR(400 MHz, DMSO-d6)δ: 7.4-7.1(m,10H,ArH), 6.5(s,1H,thiazolidine ring), 4.5& 3.91 (d,2H. thiazolidine ring.^{13}CNMR(101 MHz,DMSO-d6)δ: 175 (C=O), 145-129 (aromatic carbons), 68.3(thiazolidine ring), 39.52(Solvent DMSO).

2-(4-chlorophenyl)-3-phenylthiazolidin-4-one (T_2): Yellow precipitate**;** mp.=183°C; FT-IR cm^{-1} (KBr): 3080, 2861, 1676, 1589, 1478, 1374, 1080,913,819,750. ^{1}HNMR (400 MHz, DMSO-d6) δ: 6.7 (s,1H, thiazolidine ring), 3.89 ((d,2H,thiazolidine ring), 7.26 -7.38 (m, 8H, Ar-H). ^{13}CNMR (**0** 1MHz, DMSO-d6)δ: 169 (C=O), 136-122 (aromatic carbons),63 (CH, thiazolidine ring), 39 (DMSO),32 (CH thiazolidine ring),

2-(4-bromophenyl)-3-phenylthiazolidin-4-one (T_3): Red precipitate; mp.=57°C; FT-IR cm^{-1}(KBr): 3180,2881, 1685, 1563, 1489, 1389, 1010. ^{1}HNMR (400 MHz, DMSO-d6)δ: 7.80 -7.1 (9H,Ar-H), 6.46 (s,1H,thiazolidine ring), 3.87((d,2H,thiazolidine ring). ^{13}CNMR (101 MHz, DMSO-d6) δ: 169 (C=O), 144-129(aromatic carbon), 68(thiazolidine ring), 32(thiazolidine ring), 39(Solvent).

2-(4-hydroxy-2-methoxyphenyl)-3-phenylthiazolidin-4-one (T_4): Brown precipitate; mp.=212°C; FT-IR cm^{-1}(KBr):[24] 3443, 3092,2918,1683, 1551, 1484. ^{1}HNMR (400 MHz, DMSO-d6)δ: 9.82 (s, 1H,OH), 7.64- 6.77(8H,Ar-H), 6.71(thiazolidine ring), 4.33&4.23(d,2H,thiazolidine ring), 4.05(OCH_3) (shown in Fig. S8).^{13}CNMR (101 MHz, DMSO-d6) δ: 170.82 (C=O), 155 (C-O), 134-119 (aromatic carbons), 55.08(OCH_3), 39.5(DMSO).

3-(1,5-dimethyl-3-oxo-2-phenyl-2,3-dihydro-1H-pyrazol-4-yl)-2-phenylthiazolidin-4-one(T_5): Brown precipitate; mp. =173°C; FT-IR cm^{-1}(KBr): 3643, 3002, 2940, 2882, 1722, 1558, 1478, 1376, 1127, 1112, 829. ^{1}HNMR (400 MHz, DMSO-d6) δ7.5-7.2 (m,10H,ArH), 3.9(d,2H, CH, thiazolidine) 3.3(s, 3H, NCH_3), 2.4(s,3H,CH_3).^{13}CNMR(101MHz, DMSO-d6)δ:171(C=O)161.3(C=O), 145(CH_3/heterocyclic), 143-113 (aromatic carbons), 65 (CH thiazolidine), 39 (DMSO),36(N-CH_3), 12 (CH_3).

2-(4-chlorophenyl)-3-(1,5-dimethyl-3-oxo-2-phenyl-2,3-dihydro-1H-pyrazol-4-yl)thiazolidin-4-one(T_6): Brown precipitate; mp.=183°C; FT-IR cm^{-1} (KBr): 3531, 3100, 2991, 1691, 1554, 1443, 1371, 1113, 1080, 822, 763, 691. ^{1}H NMR (400 MHz, DMSO-d6): δ 7.6 - 7.4 (ArH), 3.9& 3.85(s, 2H, CH thiazolidine ring), 3.1 (s, 3H,CH_3), 2.31 (s, 3H,CH_3).^{13}CNMR(101 MHz, DMSO-d6)δ 165. 8(C=O), 160.55(C=O), 140-112 (aromatic carbons), 60 (CH_2S) 39 (DMSO), 34(NCH_3), 12 (CH_3).

2-(4-bromophenyl)-3-(1,5-dimethyl-3-oxo-2-phenyl-2,3-dihydro-1H-pyrazol-4-yl)thiazolidin-4-one(T_7): Brown precipitate; mp. = 216°C; FT-IR cm^{-1} (KBr): 3542, 3180, 1685, 1513,1442 1396. ^{1}HNMR (400 MHz, DMSO-d6)[29] δ: =8.09–7.48(m, 9H,Ar), 4.1(s, 2H, CH thiazolidine ring) 3.4(s, 3H,NCH_3), 2.1(s, 3H, CH_3) (shown in Fig. S9). ^{13}CNMR (101 MHz, DMSO-d6)δ:175(C=O), 167(C-N, Heterocyclic),143-115 (aromatic carbons), 133 (C-Br),63(CH_2S), 36(CH thiazolidine), 39 (DMSO), 12(CH_3).

3-(1,5-dimethyl-3-oxo-2-phenyl-2,3-dihydro-1H-pyrazol-4-yl)-2-(4-hydroxy-3-methoxyphenyl) thiazol idin-4-one(T_8): Deep yellow precipitate; mp=147°C; FT-IR cm^{-1} (KBr): 3451(OH),3250-3002(H-Ar), 2961, 1672, 1601, 1561,1532, 1493, 1361, 1132,1087, 879. ^{1}H NMR (400 MHz, DMSO-d6)δ: 11.4(1H, s, NH-C=O),) 9.5(s,1H,OH), 7.52 -7.35 (s, 6H, Aromatic -H), 6.80 (d, J = 3.8 Hz, 2H), 6.67 (s, 1H), 4.15 (s, 1H, CH thiazolidine ring), 3.8((2H, d, CH_2 thiazolidine ring), 3.11 (s, 3H,CH_3),

2.3(s, 3H,CH_3). ^{3}CNMR(101MHz, DMSO-d6)δ: 165(C=O), 160(C=O), 151-110 (aromatic carbons), 60(CH thiazolidine), 56 (CH thiazolidine), 39 (solvent), 36 (OCH_3), 12 (CH_3)

N-(2-(4-hydroxy-3-methoxyphenyl)-4-oxothiazolidin-3-yl)isonicotinamide(T_9): Brown precipitate; m.p= 123°C; FT-IR Cm^{-1}(KBr): 3458(OH), 3188, 3004, 2904,1685,1652,1564,1512,(C-S)616 (shown in Fig. S10). ^{1}H NMR (400 MHz, DMSO-d6)δ: 2.51 (H, s, CH_3), 3.2-3.83(2H, d, CH_2 thiazolidine ring), 4.5 (1H, s, CH thiazolidine ring).8-7.2(8H, m, Ar-H), 11.5 (1H, s, NH-C=O) (shown in Fig. S11). ^{13}CNMR (101MHz, DMSO-d6)δ: 169 (C=O), 164(C=O), 150-121 (aromatic carbons), 57 (CH thiazolidine),34(OCH_3) 28(CH thiazolidine) (shown in Fig. S12).

Reusability of the γ Fe_2O_3RHA@SO_3H catalyst

To demonstrate the catalyst reusability, the reaction was sequentially carried out with the catalyst at the best conditions of the reaction. For the purpose of complete conversion, the reaction was first carried out with a new catalyst. The catalysts were then filtered before being dried at a temperature of 50°C. To regenerate the catalyst, it was washed with ethanol and left to dry for one night at 60°C. Afterwards, the regenerated catalyst was ready for reuse in a new reaction round at the optimal catalytic circumstances.

Results and discussion

Element analysis of catalyst by EDX

The elemental composition of RHA and the nanomagnetic catalyst was determined by EDX and elemental analysis techniques. The elemental analysis measurements data of γ Fe_2O_3RHA@SO_3H, γ Fe_2O_3RHA, and RHA (silica) are summarized in Table 1. The percentage of sulfur in γ Fe_2O_3RHA@SO_3H was 1.30 wt%, while the EDX results showed that this element percentage was11.05 wt% in γ Fe_2O_3RHA@SO_3H. In addition to S, the EDX spectrum of the catalyst exhibited the presence of Fe, and O elements as shown in Fig. 1.

This confirms that the (-O_3SOH) moiety was successfully attached to the Fe_2SiO_n, where the nanomagnetic catalyst consisted of 37.82 wt %O, 3.25 wt %Si, 0.1 wt % C, and 22.98 wt % Fe. The combination of Fe, silica and -O_3SOH in the formed catalyst led to a fully-developed porous arrangement, which is thought to have a significant role in enhancing its activity. It was noticed that the existence of S resulted in a high acidity of the formed catalyst, which can improve the amine- aldehyde condensation to generate Schiff bases. Similarly, the high level of O indicates that the produced metallic and synergistic molecules that contain oxygen atom are primarily attached to the Fe, Si, S composite instead of being attached to separate metal oxide species. Temperature Programmed Desorption (TPD) was used to ascertain both the acidic and basic features of RH, RHA, γ

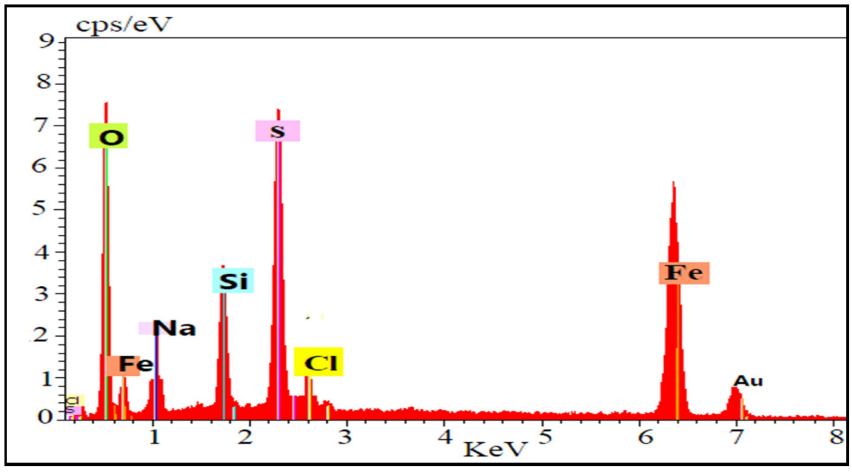

Fig. 1. EDX spectra of the catalyst γ Fe_2O_3RHA@SO_3H.

Table 1. EDX analysis of γ Fe_2O_3RHA@SO_3H and RHA.

Entry	O	H	Si	S	Fe	C
γ Fe_2O_3RHA@SO_3H	37.82	–	3.25	11.05	22.98	0.1
RHA	–	1.6	29.09	–	–	0.84

Table 2. Total desorption and textural features of carbon dioxide and ammonia for RH, RHA, γ Fe_2O_3RHA and γ Fe_2O_3RHA@SO_3H.

Entry	Specific surface area *BET* (m2 g^{-1})	TPD-CO Total Basicity (mmolg^{-1})	TPD-NH_3 Total Acidity (mmolg^{-1})	Schiff base (%)[a]
RH	3.97	2.04	15.57	No .reaction
RHA	347	2.66	37.34	No reaction
γ Fe_2O_3RHA	202	3.34	37.38	66.9
γ Fe_2O_3RH@SO_3H	193.12	2.41	42.87	94

a Reaction condition (non-optimized): ethanol solvent, 5% catalyst, 70°C temperature, 1h reaction time.

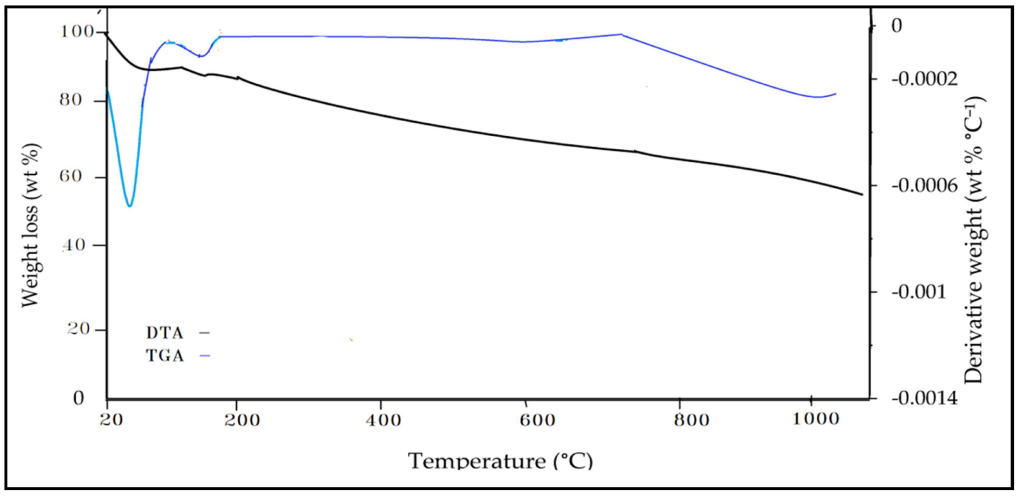

Fig. 2. Thermograph of nano-catalyst γ Fe_2O_3RHA@SO_3H.

Fe_2O_3RHA and γ Fe_2O_3RHA@SO_3H (obtained from silica) through carbon dioxide and NH_3–TPD as illustrated in Table 2. According to the findings, the catalysts obtained from rice husk exhibited bifunctional features as they comprised both basic and acid spots. They also showed a good desorption of CO_2 and NH_3 at different temperatures, which designate the strength level of basicity and acidity of the catalysts. Commonly, the acidity and basicity strength of γ Fe_2O_3RHAand γ Fe_2O_3RHA@SO_3H appeared to be feeble to moderate at total desorption, where the basic density was 2.04 mmol g^{-1}, 2.66 mmol g^{-1}, and the acidic density was 15.57 mmol g^{-1}, 37.43 mmol g^{-1}, respectively. Moreover, doping the rice husk ash by $FeCl_3$ and $FeCl_2$ (to form Fe_2O_3) resulted in a significant increase in the entire basicity and acidity strength. On the other hand, analysis of TPD-CO_2 displayed that the CO_2 desorption was at a temperature range of 550 - 820°C. The maximum temperature range of this desorption was 702-778°C, which indicates the high strength of basic spots generated from SiO_2 and Na_2O. Similarly, the catalysts acidity arising from loading of H_2SO_4 on γ Fe_2O_3RHA resulted in an increase in the total desorption of NH_3. Nevertheless, doping of γ Fe_2O_3RHA with 5% H_2SO_4 resulted in lessen its basicity, as the basic spots in the catalyst were inhibited by H_2SO_4, and subsequently allowing the Schiff bases to convert into the products. In addition, scattering of the surplus clusters of Fe on the surface of RHA could reduce its surface support and the catalyst pore size, consequently diminishing the RHA porosity, which causes a reduction in the surface of BET.[25] It was noticed that the Schiff bases yield is significantly affected by the catalyst acidity. The high catalyst acidity resulted in producing the biggest amount of the Schiff base as displayed in Table 2, where the highest yield of γ Fe_2O_3RHA@SO_3H was obtained compared to the other catalysts. Accordingly, the magnetic nano-catalyst was selected for an additional description and catalytic optimization in the formation of Schiff bases.

Thermogravimetric analysis (TGA)

The thermal stability of the nano-catalyst was ascertained using thermogravimetric analysis (TGA). Fig. 2 shows four essential stages of thermal decomposition. The first sage involved a loss of (17.01%) from the sample weight at a temperature range of 25- 162°C, which could be due to the elimination of the adsorbed H_2O molecules (physical adsorption and chemical adsorption). The second stage was the primary pyrolysis at a temperature of 180 -227°C, with a weight loss of 2.43%, which is ascribed to the

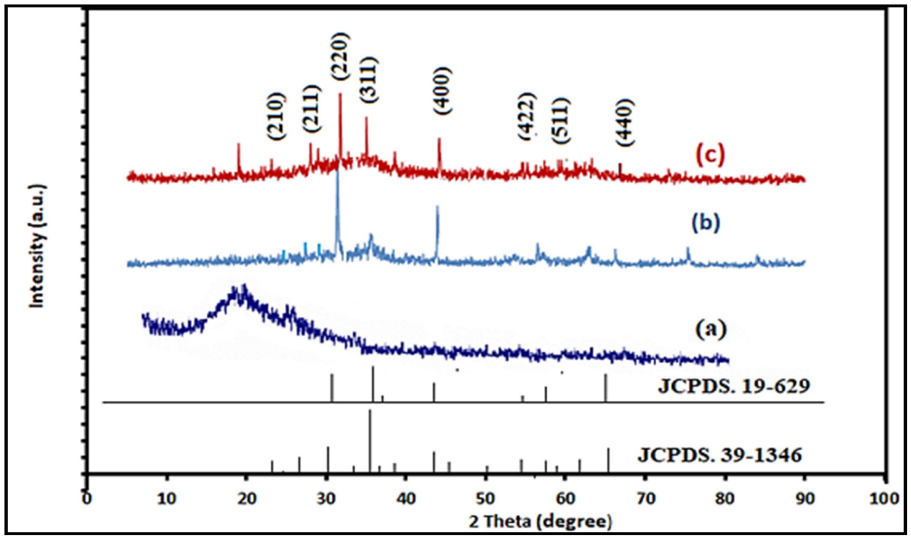

Fig. 3. XRD diffraction patterns of silica (RHA)(a),γFe_2O_3RHA(b) and γFe_2O_3RHA@SO_3H catalyst (c).

Table 3. The values of the inter plane distances calculated from XRD of γ Fe_2O_3RHA (b) and γ Fe_2O_3RHA@SO_3H catalyst (c).

Sample	2theta (Deg.)	FWHM(Deg.)	Dhkl Exp.A°	(C.s)cm)
γ Fe_2O_3RHA (b)	19.0017	0.0806	4.6667	100.0
	33.7546	0.08966	2.6533	9.3
	33.7546	0.7227	2.6533	11.5
	48.7821	0.1916	1.8653	45.5
	28.2217	2.0034	3.1596	4.1
γ Fe_2O_3RHA@SO_3H	31.7581	0.1959	2.8153	42.2
catalyst (c).	45.5035	0.2387	1.9918	36.1
	33.6169	0.1121	2.6638	74.0
	57.1141	0.1129	1.6114	80.1
	62.8738	0.6810	1.4769	13.7
	75.4868	0.4339	1.2584	23.2
	75.4868	0.8400	1.2584	12.0

OH ions dihydroxylation of –SO_3H group. The third stage of decomposition was at a temperature ranging from 200˚C to 650˚C ans is assigned to Fe_2O_3 groups. The last stage of decomposition was at a temperature above 800˚C with a major weight loss of (20.11%), which ascribed to the Si-O-Si bonds, as shown in Fig. 2.

XRD diffraction of γ Fe_2O_3RH@SO_3H nanocatalyst

The X-ray diffraction (XRD) pattern of the prepared silica from rice husk (RH) and the super magnetic γ Fe_2O_3RH@SO_3H nano-catalyst is shown in Fig. 3 and the diffraction peaks were recognized employing the standard JCDPS file. A broad diffraction peak within 12.0˚ - 30˚ for RH is assigned to amorphous silica. After the loading of $FeCl_2$ and $FeCl_3$ in a (1:1) molar, the intensity of the chief broad peak of RH reduced regularly and a new peaks presented in the XRD pattern. Some of the peaks appeared in the region of 30.3˚, 35.7˚, 43.3˚, 53.7˚, 57.3˚, 62.9˚ and 74.6˚ correspond to 220, 311, 400, 422, 511, 440 and 533 phases of the Fe_2O_3,[26] and Fe_3O_4 due to the high similarity between both patterns. Likewise, the same results were obtained when the experimental values were compared with their corresponding values of standard magnetite (JCPDS file no. 39-1346) and magnetite (JCPDS file no. 19-629) records, where the experimental data are too similar to their corresponding of JCPDS file no. 39-1346 of magnetite. The XRD pattern of the as-synthesized γ-Fe_2O_3 nanoparticles discloses that the γ-Fe_2O_3 peaks are located in the range from 20˚ to 30˚. That is to say, these particles comprise iron oxides, Fe_2O_3 and Fe_3O_4, but Fe_2O_3 is the predominant cubic and tetragonal phase, respectively. On the other hand, the combination of Fe_3O_4, Fe_2O_3 and SiO_2 materials on the catalyst throughout the calcination gave rise to both of those peaks.[27]

Furthermore, the Debye–Scherrer equation was utilized to assess the average crystallite size of the

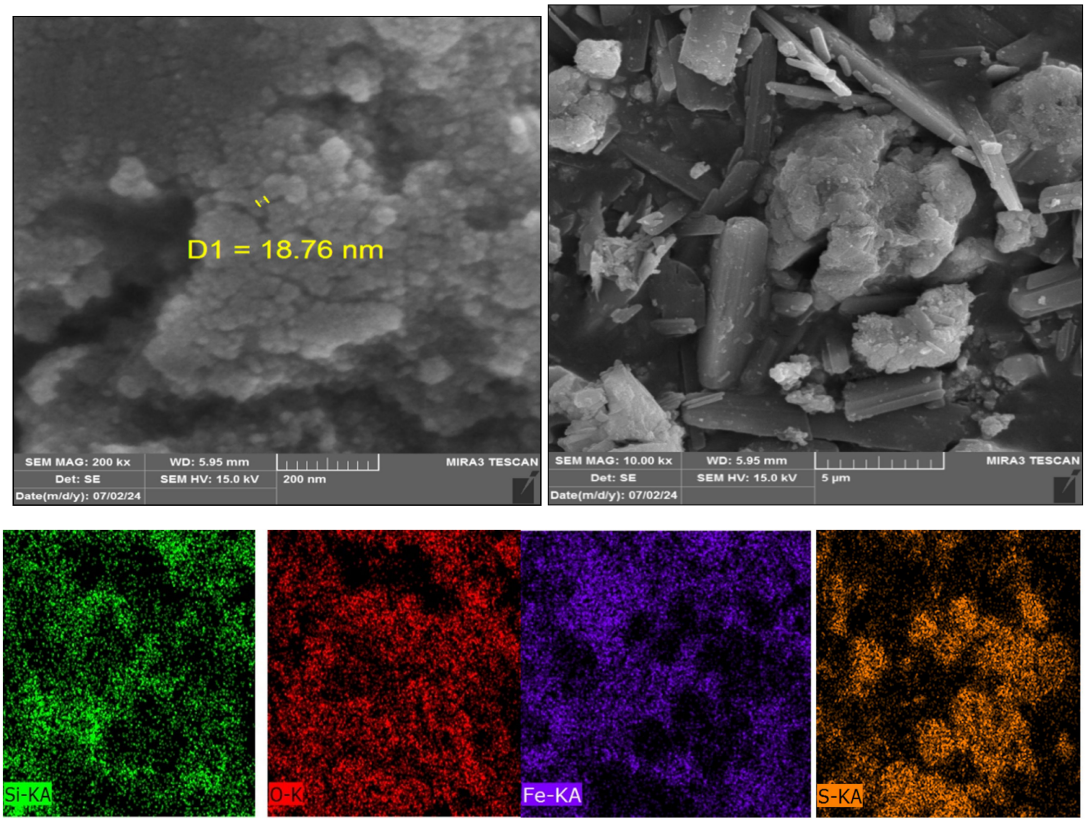

Fig. 4. FESEM images of the nano-catalyst γ Fe_2O_3RHA@SO_3H, and elemental mapping images of Si, O, Fe, and S, respectively.

catalyst, as shown in Table 3. In the range of 23–75 nm, a normal drop was observed. This is well-aligned with the sizes detected in TEM measurements. The generation of crystalline nanoparticles of Fe_2O_3 with a clearly described Face-Centered Cubic arrangement was confirmed by the XRD findings.

Scanning electron microscopy

FESEM study was conducted to test the morphology profile of silica and the catalyst. The FESEM measurement data demonstrated that there was an accumulated-layer mineral formed of ordered parts on the amorphous silica surface in Fig. 4. The Fe_2O_3 formed through the sol-gel method commonly possesses a tube shape.[28] The size of the generated nanoparticles was 18.76 nm. EDX was utilized to test the elemental profile of γ Fe_2O_3RHA@SO_3H. The EDX-graphs display the important elements including Si, O, Fe, and S, which are presented in the silica matrices as shown in Table 1. Thus, Fe_2O_3 NPs immobilization on the surface and within interlamellar gaps of silica was effectively established according to these tests. As observed in Fig. 4, the distribution of Si, Fe, S, and O was homogeneous. This designates that these elements were distributed over the catalyst in a uniform way. Hence, the FESEM/EDX results confirm the immobilization of Fe_2O_3 and $HOSO_3$ on the amorphous silica surface, which agrees with the XRD data. Moreover, TEM images were taken to show the shapes and arrangements of the catalyst, which revealed that the particle size of Fe_2O_3 ranged from 7 to 40 nm with regular scattering over the silica as illustrated in Fig. 5. Figs. 4 and 5 show the FE-SEM and TEM micrographs of γ Fe_2O_3RHA@SO_3H, which revealed the presence of aggregated particles that can be associated with its highly porous nature resulting in a high surface area. Fig. 4 shows that the nanocatalyst was built from the aggregation of asymmetrical particles with different sizes. Some of these aggregates have cylinder shape, which mostly belongs to the iron oxide bound to the permeable surface of the silica forerunner.

Vibrating sample magnetometer (VSM) measurements

The magnetic action of silica, Fe_2O_3RHA, and γFe_2O_3RHA@SO_3H was examined at ambient temperature exploiting a vibrating sample magnetometer (VSM) as displayed in Fig. 6. The magnetization of pristine Fe_2O_3-RHANPs and the catalyst

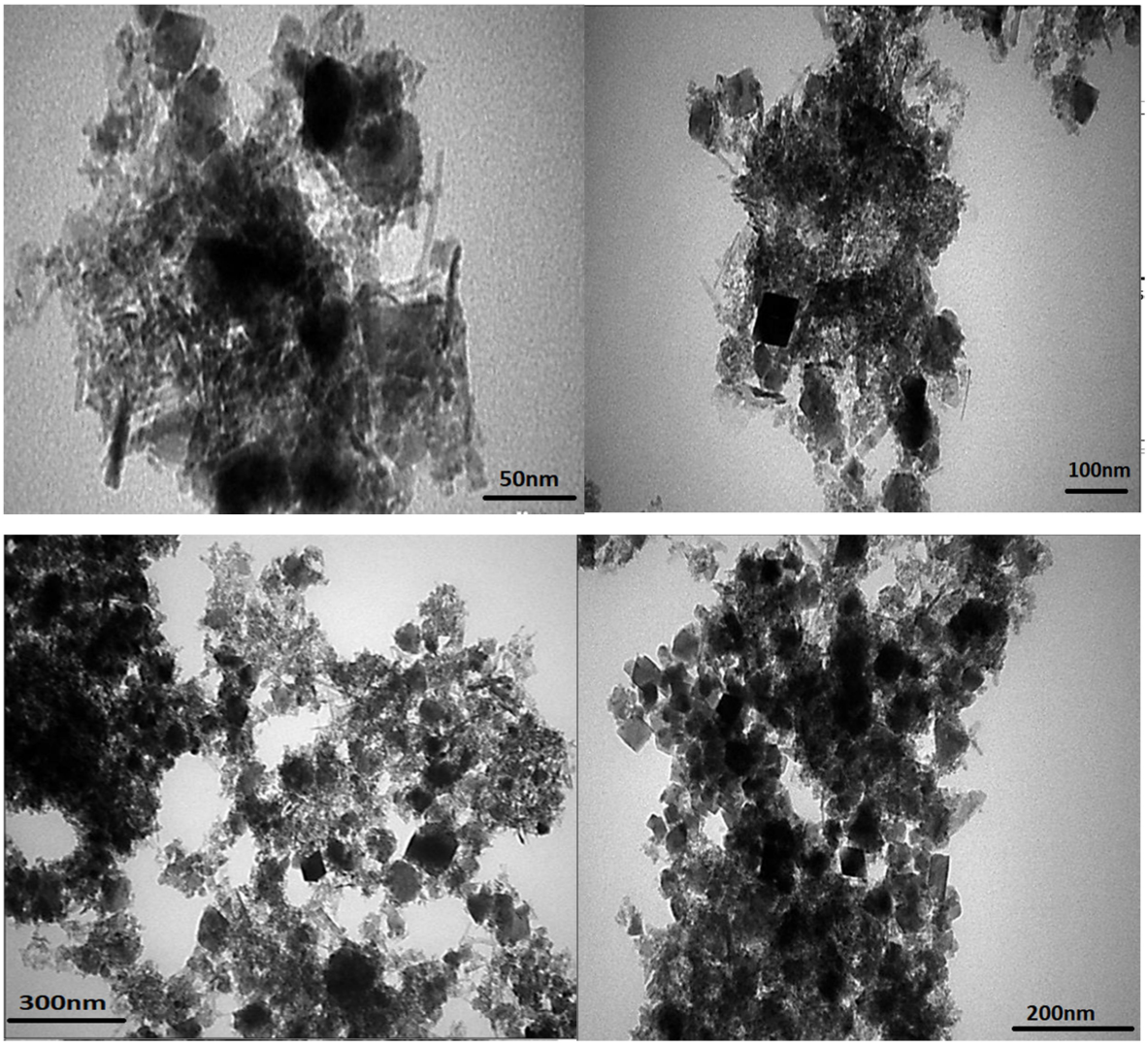

Fig. 5. TEM images of the γ $Fe_2O_3RH@SO_3H$ nanoparticles at different magnifications.

($\gamma Fe_2O_3RHA@SO_3H$) was about 5.7 (emu/g). The values of silica saturation magnetization about zero emu\g based on measurements from VSM. The drop in saturation magnetization level is attributed to H_2SO_4 incorporation on Fe_2O_3-silica, which demonstrates the formation of the nanocomposite. This is a desirable magnetic characteristic as it facilitates the easy separation of the nanocomposite from the reaction solution after being subjected to an applied magnet.

Catalytic Study of $\gamma Fe_2O_3RHA@SO_3H$

Evaluation of the activity of the heterogeneous catalysts $\gamma Fe_2O_3RH@SO_3H$ to create Schiff bases through the combination of various aromatic aldehydes with various primary aromatic amines is one of this work targets.[29] The general reaction is explained in Scheme 1. Aiming to optimize the reaction conditions, several reaction parameters were assessed. These parameters include the sort of reaction solvents, reaction time, the reaction temperature, and the catalyst amount used for the preparation of the Schiff base. Also, the mechanism of the catalyst and the catalyst usability were studied. As illustrated in the following sections, the yield and rate constants were evaluated as well.

Impact of reaction time

The impact of reaction time on the synthesis of Schiff base over the $\gamma Fe_2O_3RHA@SO_3H$ surface is illustrated in Table 4. The reaction was conducted using 0.05 g of catalyst at 70°C. Within the first half an hour of the reaction, the amount of Schiff base produced was 63%. Then, in 2.5 hours, the yield

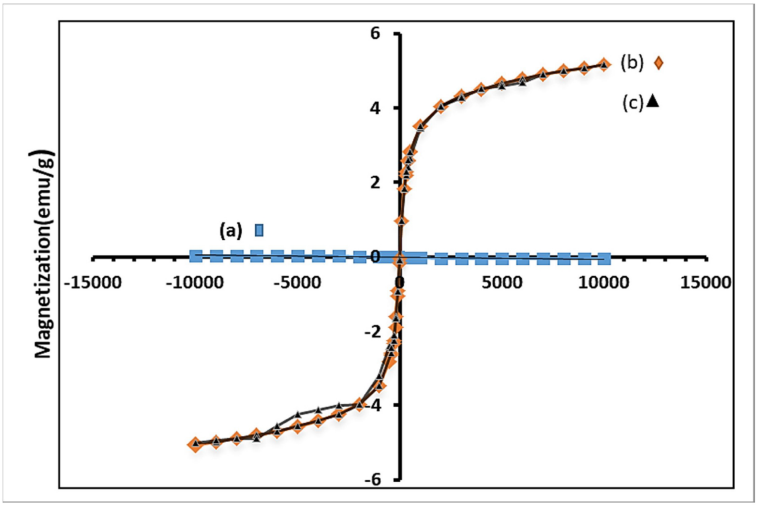

Fig. 6. Magnetization curves of (a) silica, (b) γFe_2O_3 /RHA and (c) $\gamma Fe_2O_3RH@SO_3H$ nanocomposite.

Table 4. The effect of some parameters on the Schiff base (N,1-diphenylmethanimine) yield.

Parameters	Variants	product yield%	Parameters	Variants	product yield%
	0.5	70	Temp.°C	32	-
	0.5	70		45	23
	1	86		50	29
Time, h	1.5	90		60	45.3
	2	91		65	87
	2.15	94		70	94
	3	94			
Mass of catalyst, g	0.05	94	Solvent	Ethanol	94
	0.1	90		Propanol	53.5
	0.15	84		Butanol	32

increased to reach up to 90%. However, after 11 hours of the reaction time, there was no sign of forming more amount of Schiff base. This indicates that 2.5 h is the optimal time for the Schiff base preparation. The activity of $\gamma Fe_2O_3RHA@SO_3H$ is attributed to the existence of active spots represented by sulfate segments, which play a critical function throughout the reaction.

The catalyst mass impact

The synthesis of Schiff bases was achieved using a variety of amounts of $\gamma Fe_2O_3RHA@SO_3H$ (0.05–0.2 g) and the other conditions remained constant (2.5 h as the reaction time and 70˚C as the temperature of the reaction). Table 4 shows the obtained data. When the catalyst mass of $\gamma Fe_2O_3RHA@SO_3H$ decreased from 0.2 to 0.05 g,[29] the formed amount of Schiff base raised by 14% (from 70 to 94 %). Furthermore, the surface area was affected significantly by the change in the catalyst mass, where the surface area decreased as the catalyst mass increased. Likewise, increasing the catalyst mass leads to an increase in conversion. The reason behind that is the plenty of catalytically active sites available. Hence, the optimal catalyst mass chosen was 0.05 g.

Temperature impact

Table 3 displays the impact of the reaction temperature on the synthesis of Schiff base. When the temperature was raised by 20˚C (from 50 to 70˚C), the created amount of Schiff base noticeably raised from 23 to 94 %. Increasing temperature could lead to a raise in the assembly of the reaction materials over the catalyst, resulting in raising the reaction rate, and consequently increasing the amount of the produced bases. It is worth mentioning that a study of the effect of increasing temperature was not conducted for temperatures close to or more than the solvent boiling point.

Solvent impact

Table 4 describes the impact of solvents (alcohols) that were utilized as reaction media for the preparation of Schiff bases. Over $\gamma Fe_2O_3RHA@SO_3H$, the reaction between benzaldehyde and aniline was

Table 5. The impact of recycled catalyst on the yield of the formed Schiff bases.

Variants	Product yield%
Fresh	94
1	94
2	90
3	83

investigated at the optimal circumstances. Ethanol, 1-propanol, and 1-butanol) were used as the reaction solvents. It was found that the produced amount of the bases was ordered as follows: 1-butanol < 1-propanol < ethanol.[30] This demonstrates that there is an inverse proportion between the number of carbon atoms and the product yield.

The catalyst recycling

Upon the recovery of the catalyst, its catalytic ability was examined. The relationship between the recycled catalyst, $\gamma Fe_2O_3RHA@SO_3H$, and the bases yield is displayed in Table 5. It can apparently be noticed that the activity of the catalyst has not changed, which demonstrates the high stability of the catalyst throughout the reaction. As the condensation reactions between different aldehydes and aniline or 4-amino-antipyrine produce Schiff bases.[31] The catalytic activity of $\gamma Fe_2O_3RHA@SO_3H$ in these reactions was investigated, and the data are described in Table 6. It can apparently be seen that the catalyst has high activity and can efficiently be utilized for the creation of Schiff bases analogs with high yield percentages. More than 73-94% yield of Schiff bases analogs was obtained from all the examined reactants in the experiments.

Comparing synthesized nano-catalysts with different solid-acid catalysts

The creation method of 1,3-Thiazolidin-4-one analogs from Schiff base and mercaptoacetic acid was compared to other procedures in which acidic catalysts were utilized. The purpose of this comparison is to evaluate the properties and border of this system (1,3-Thiazolidin-4-one). This is an effective way for the synthesis of 1,3-Thiazolidin-4-one analogs under simple circumstances, as no solvent was used and the reusability of the nano-catalyst even after being recycled three times. As compared to other catalysts, a fast reaction was observed, and a high yield was obtained when $\gamma Fe_2O_3RHA@SO_3H$ was utilized to produce 1,3-Thiazolidin-4-one derivatives (T_1-T_9), as shown in Table 7. The synthesis of Schiff base compounds (S_1-S_9) was achieved via the reaction of aromatic amine/anisonicotinic acid hydrazide with aromatic aldehydes in the presence of the nano-catalyst and using ethanol as a solvent. As illustrated in Scheme 1, the synthesis of Schiff bases (S_1-S_9) involves the nucleophilic addition to the carbonyl group of the aromatic aldehyde in the presence of an acidic catalyst. An attack by the amine group (acting as a nucleophile) occurs at the intermediate carbocation, where a molecule of H_2O is eliminated leading to the creation of an imine moiety. The general procedure to prepare the compounds is explained in Scheme 1. The FT-IR spectra of Schiff bases (S_1-S_9) showed the appearance of new absorbance bands at (1591-1625) cm^{-1} due to the imine group (C=N). All data of the prepared compounds are shown in section 2.7. On the other hand, the ^{1}HNMR spectra of compounds (S_1-S_9) disclosed singlet signals at (8.39, 7.41, 7.8, 8.8, 8.7, 8.7, 9.5, 9.5 and 8.3 ppm assigned to the imine protons (HC=N), which confirms the formation of Schiff base compounds as shown in section 2.7. ^{13}CNMR spectra of compounds (S_1-S_9) showed signals at (166,167,159,166,137.44,148,149, 148.7 and 148 ppm) belonging to (C=N) group.

The synthesis of the desired thiazolidine compounds (T_1- T_9) was attained via the reaction of Schiff bases (S_1-S_9) with mercaptoacetic acid in the presence of the nano-catalyst, solvent-free, with stirring in a microwave. The FT-IR spectra of the prepared 1,3-thiazolidine-4-one compounds (T_1-T_9) showed the presence of new bands at (1722-1683)cm^{-1} belonging to the carbonyl C=O of the thiazolidine ring. Also, the appearance of new absorption at υ(690-616) cm^{-1} due

Table 6. The percentages of Schiff bases yield at the optimized conditions of the reaction.

Entry	Variants	Product yield%
S_1	Benzaldehyde + aniline	94
S_2	p-Chloro-benzaldehyde + Aniline	91
S_3	p-Bromo-benzaldehyde + Aniline	95
S_4	Vanillin + Aniline	87
S_5	Benzaldehyde + 4-aminoantipyrine	73
S_6	p-Chloro-benzaldehyde + 4-aminoantipyrine	80
S_7	p-Bromo-benzaldehyde + 4-aminoantipyrine	82
S_8	Vanillin + 4-aminoantipyrine	77
S_9	Isonicotinohydrazide + Vanillin	81

Table 7. Synthesis of 1,3-thiazolidin-4-one derivatives using nano- γ Fe_2O_3RHA@SO_3H.

Entry	Schiff base	Product	Yield %
S_1	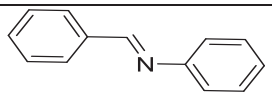	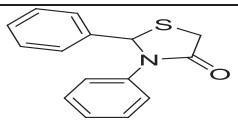 T_1	87
S_2	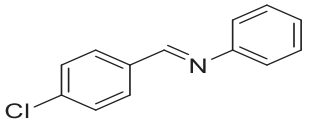	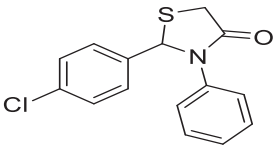 T2	91
S_3	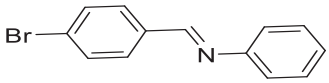	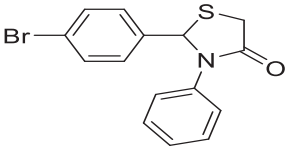 T_3	90
S_4	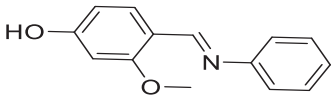	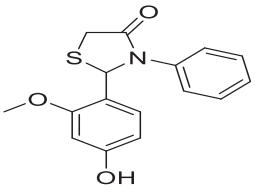 T_4	67
S_5	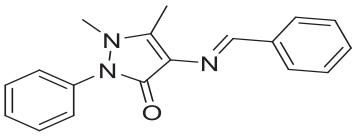	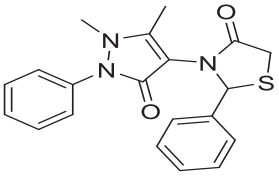 T_5	81
S6	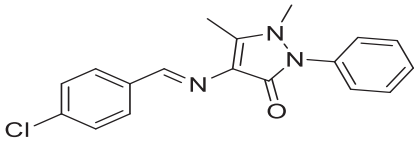	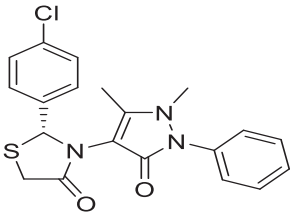 T_6	90
S_7	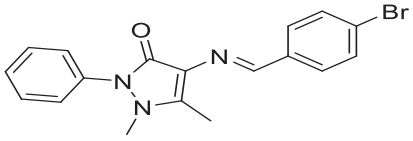	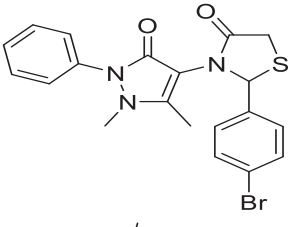 T_7	89
S_8	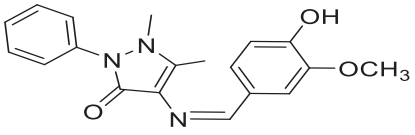	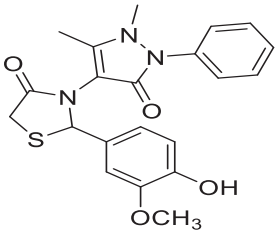 T8	66
S_9	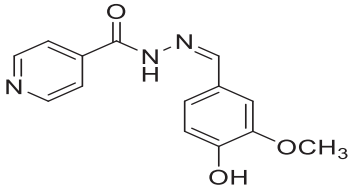	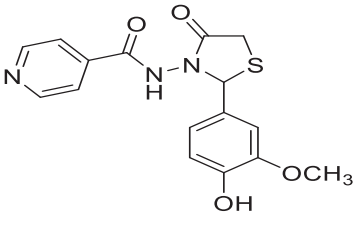 T_9	53

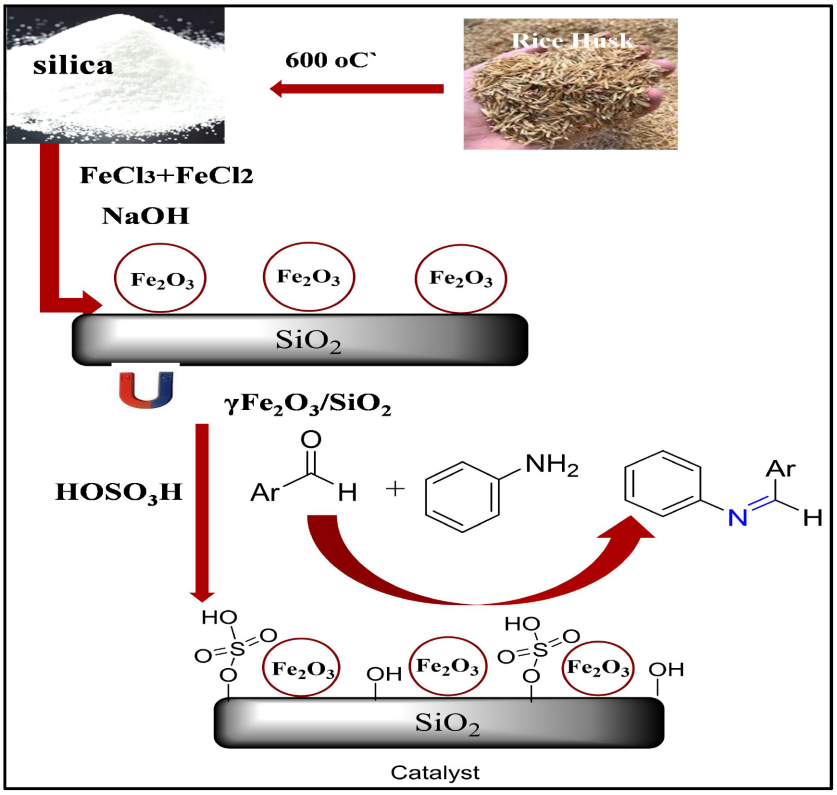

Scheme 1. Synthesis of the catalyst and Schiff bases reaction on the surface of γ Fe_2O_3RHA@SO_3H.

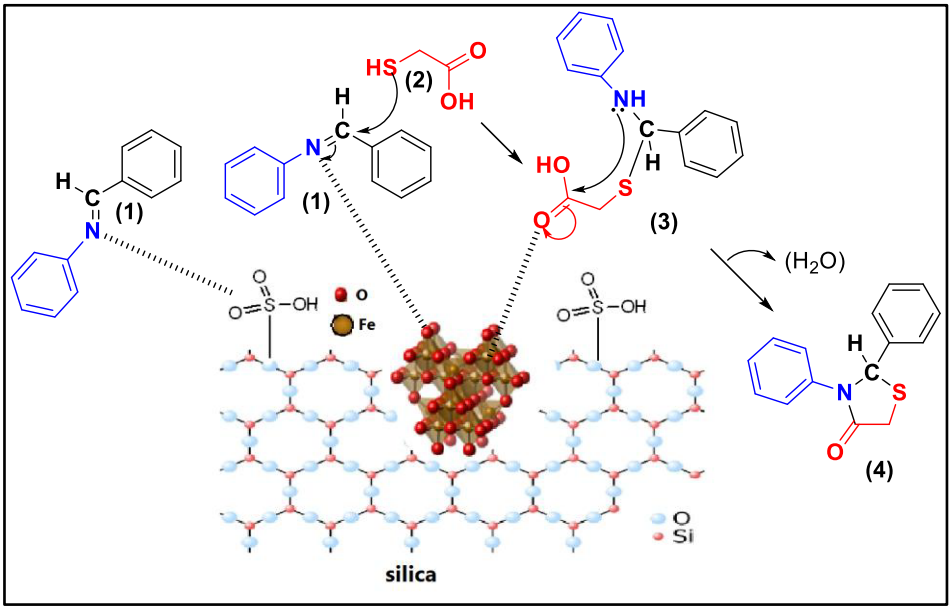

Scheme 2. The suggested mechanism for the creation of 1,3-thiazolidin-4-one derivative.

to C-S of the thiazolidine ring). ^{1}HNMR spectra data of the derivatives (T_1- T_9) showed the disappearance of the singlet signal of HC=N proton of Schiff bases. Moreover, the appearance of a singlet signal at 6 ppm ascribed to (N-CH) of thiazolidine ring, and presence of (d-d) signals at (4.1-3.9 ppm) are attributed to ($S-CH_2$) of thiazolidine ring.[31–33] This confirms the cyclization process and synthesis of the desired compounds.

The suggested mechanism for the creation of a 1,3-thiazolidin-4-one derivative is explained in Scheme 2. The Schiff base (1) attaches with the

Table 8. Formation of 1,3-Thiazolidin-4-one derivatives with different solid acid catalysts.

Nanocatalyst	Time (min)	Temperature (°C)	Solvent	Yield (%)	Ref.
γ Fe_2O_3RHA@SO_3H	20	90	free	53–90	This work
$CuFe_2O_4$@MT(CuF@MT)(0.025 g)	25	90	free	74–90	[34]
Pd nanoparticles (10 mol%)	60	100	free	65–90	[35]
SiO_2 (0.5 g)	420	25	DCM	78	[36]
$Bi(SCH_2COOH)_3$ (10 mol%)	120	70	free	75	[37]
Y_2O_3 particles (2 mol%)	60	25	free	87	[38]
Montmorillonite k10 (0.5 g)	360	50	DMF	65–97	[39]
Montmorillonite k10 (0.5g)	360	120	DMSO	60	[39]
mMWCNT (0.1 g)	60–120	25	free	82–92	[40]
Ni@zeolite-Y(10% Wt)	25	25	EtOH	80–95	[41]
ZnO–NiO–$NiFe_2O_4$ (0.025g)	60–180	100	DMF	74–96	[42]
2-Oxoimidazolidine-1,3-disulfonic acid (OImDSA)	90	free	free	84–90	[43]

catalyst (γ Fe_2O_3RHA@SO_3H) through hydrogen bonding. Whereas, the imine in Schiff base is attacked by the sulfur atom of mercaptoacetic acid (2) to form an intermediate (3). Afterwards, the formed intermediate is subjected to an intramolecular cyclization via the elimination of an H_2O molecule to produce 1,3-thiazolidin-4-one derivative (4).

To assess the benefits and restrictions of the present system in the formation of 1,3-thiazolidin-4-one, the generation of 1,3-thiazolidin-4-one derivatives from Schiff base and mercaptoacetic acid was compared with various other solid acid catalysts utilized in earlier published works Table 8. In comparison with those catalysts, the current procedure in synthesizing 1,3-Thiazolidin-4-one derivatives under simple reaction environments is an excellent alternative. This is attributed to several reasons: The catalyst recyclability after at least three successive reaction runs, a remarkable product yield, and a high reaction rate Table 8.

Conclusion

In this research paper, Fe_2O_3 was efficiently immobilized onto silica derived from rice husk and then sulfonated by dilute sulfuric acid, affording a nanocatalyst labeled as γFe_2O_3RHA@SO_3H. The created nano-catalyst showed effective superparamagnetic characteristics, allowing simple separation and recovery using a magnet. The recycling experiments demonstrated that the prepared nano-catalyst retained its activity and can be remarkably recycled many times to produce Schiff bases and 1,3-Thiazolidin-4-one derivatives. This is an effective approach for providing favorable features, including facile reaction circumstances, cheap reactants, time saving, noteworthy product yield, simple separation process, and most importantly, it fulfills green chemistry conditions. In summary, the synthesized γFe_2O_3@RHA–SO_3H is a recoverable, reusable, environmentally friendly, and acidic nano-catalyst with promising potential for various chemical conversions.

Acknowledgment

The authors thank College of Science/Wasit University for using their facilities to conduct this work.

Authors' declaration

- Conflicts of Interest: None.
- We hereby confirm that all the Figures and Tables in the manuscript are ours. Furthermore, any Figures and images that are not ours have been included with the necessary permission for republication, which is attached to the manuscript.
- No animal studies are present in the manuscript.
- No human studies are present in the manuscript.
- Ethical Clearance: The project was approved by the local ethical committee at University of Waist.

Authors' contributions statement

A.G. S contributed to the design; J.K.A., A.G. S., and Z.R.K. contributed to the implementation of the research, the analysis of the results, and the writing of the manuscript. All authors have read and agreed to the final draft of the manuscript.

Data availability

Data are available upon reasonable request and will be provided by the corresponding author.

Supplementary materials

Supplementary materials are available at https://doi.org/10.21123/2411-7986.5274.

References

1. Deise TP, Giovani JB, Eduardo PK, Francisco DR. Rice husk ash as an alternative soluble silica source for alkali-activated metakaolin systems applied to recycled asphalt pavement

stabilization. Transport Geotech. 2023;39:100940. https://doi.org/10.1016/j.trgeo.2023.100940.
2. Deivaseeno D, Nisha G, Sarani Z, Ratnam W. Green synthesis and characterization of UKMRC-8 rice husk-derived mesoporous silica nanoparticle for agricultural application. Sci Rep. 2022;12:20162. https://doi.org/10.1038/s41598-022-24484-z.
3. Raymond WS, Biraja PM, Swagato D. Performance of rice husk ash (RHA) and recycled coarse aggregate(RCA) for sustainable concrete: a review. Next Mater. 2025;8:100778. https://doi.org/10.1016/j.nxmate.2025.100778
4. Niculescu V-C, Raboaca MS. Efficient Rice-husk-derived silica nanocatalysts for organic dye removal from water. Catalysts. 2021;11(7):815. https://doi.org/10.3390/catal11070815.
5. Hafez AI. Synthesis of silica and silica compounds based on rice husk ash. Wat Ener Food Env J. 2022;2:67–75. http://dx.doi.org/10.18576/wefej/030203.
6. Elise OB, Vedrana AD, Peter SJ. A physical model for microstructural characterization and segmentation of 3D tomography data. Mater Charact. 2021;171:110796. https://doi.org/10.48550/arXiv.2009.07218
7. Doukeh R, Râpă M, Matei E, Prodan D, Győrgy R, Trifoi A, Banu I. An evaluation of glycerol acetalization with benzaldehyde over a ferromagnetic heteropolyacide catalyst. Catalysts. 2023;13(4):782. https://doi.org/10.3390/catal13040782.
8. Wang H, Zhang C, He H, Wang L. Glucose production from hydrolysis of cellulose over a novel silica catalyst under hydrothermal conditions. J Environ Sci. 2012;24:473–478. https://doi.org/10.1016/S1001-0742(11)60795-X.
9. Kasim M H, Hayder H M, Mosa J M, Mahmood SM. Hydrolysis of cellulose over silica-salicylaldehyde phenylhydrazone catalyst. J Taiwan Inst Chem Eng. 2015 Jan;46:74–81. https://doi.org/10.1016/j.jtice.2014.09.005.
10. Mustafa M, Hasan AL, Abbas AN, Asim AB. Green synthesis of 1,3-thiazolidin-4-ones derivatives by using acid-activated montmorillonite as catalyst. Inorg Chem Commun. 2024;161:112076. https://doi.org/10.1016/j.inoche.2024.112076.
11. Govan J, Gun'ko YK. Recent advances in the application of magnetic nanoparticles as a support for homogeneous catalysts. Nanomater. 2014;4(2):222–241. https://doi.org/10.3390/nano4020222.
12. Prateek KP, Harshita S. Synthesis, characterization and catalytic activity of GO/ZnO nanocomposite for green synthesis of dihydropyrimidinones/thiones as potential antibacterial agents. Inorg Chem Commun. 2025;181:115026. https://doi.org/10.1016/j.inoche.2025.115026.
13. Figueiredo V V, Bonfim RPF, Silva MA, Moreira CA, Pérez G AC, Lourenço WA, *et al.* Iron oxide nanoparticles: Synthesis, surface reactivity and transformative behavior under methane reducing atmosphere study via in situ XRD. Mater Chem Phys.2025;337:130564. https://doi.org/10.1016/j.matchemphys.2025.130564
14. Mustafa MHA, Abbas Al-N, Asim AB, Gamal A El-H. Organic synthesis via renewable heterogeneous nanocatalysts based on montmorillonite clay. Curr Org Chem. 2024;28(3):213–221. https://doi.org/10.2174/0113852728294884240105073842.
15. Adeeyo AO, Alabi MA, Oyetade JA, Nkambule TTI, Mamba BB, Oladipo AO, Makungo R, Msagati TAM. Magnetic nanoparticles: advances in synthesis, sensing, and theragnostic applications. Magnetochemistry. 2025;11(2):9. https://doi.org/10.3390/magnetochemistry11020009.
16. Stiufiuc GF, Stiufiuc RI. Magnetic Nanoparticles: Synthesis, characterization, and their use in biomedical field. Appl Sci.2024;14(4):1623. https://doi.org/10.3390/app14041623
17. Athra GS, Jawad KA, Zeena R K. Synthesis of dyes sulfamidazole: characterization, evaluation, molecular docking and global descriptors by density functional theory (DFT). Karbala Int J Mod Sci. 2024;10:286–296. https://doi.org/10.33640/2405-609X.3353.
18. Mustafa M H A, Abbas A, Asim AB. Montmorillonite clay modified by $CuFe_2O_4$ nanoparticles, an efficient heterogeneous catalyst for the solvent-free microwave-assisted synthesis of 1,3-thiazolidin-4-ones. Res Chem Int. 2024 Feb;50:1541–1556. https://doi.org/10.1007/s11164-024-05231-7.
19. Duha MH, Kassim M, Aqeel M, Hasanain GJA, Haider RS, Hussein AKK. Silica-coated zinc oxide nanocomposite: a novel green synthesis using rice husk as a source of silica nanoparticles. Phosphorus Sulfur Silicon Relat Elem. 2026;201(3):263–71. https://doi.org/10.1080/10426507.2025.2591728
20. Nadia B, Ahmed AA, Waleed KA, Wan NRWI. Corrosion inhibition properties of schiff base derivative against mild steel in HCl environment complemented with DFT investigations. Sci Rep. 2023 Jun 2;13(1):8979. https://doi.org/10.1038/s41598-023-36064-w.
21. Ceramella J, Iacopetta D, Catalano A, Cirillo F, Lappano R, Sinicropi MS. A review on the antimicrobial activity of Schiff bases: Data collection and recent studies. Antibiotics. 2022 Feb 1;11(2):191. https://doi.org/10.3390/antibiotics11020191.
22. Tsantis ST, Tzimopoulos DI, Holynska M, Perlepes SP. Oligonuclear actinoid complexes with schiff bases as ligands—older achievements and recent progress. Int J Mol Sci. 2020;21:555. https://doi.org/10.3390/ijms21020555.
23. Abdel-Rahman LH, El-Khatib RM, Nassr LAE, Abu-Dief AM, Ismael M, Seleem AA. Metal based pharma-cologically active agents: synthesis, structural characterization, molecular modeling, CT-DNA binding studies and in vitro antimicrobial screening of iron(II) bromosalicylidene amino acid chelates. Spectrochim Acta. 2014;117A:366–378. https://doi.org/10.1016/j.saa.2013.07.056.
24. Safaei-Ghomi J, Shahbazi-Alavi H, A flexible one-pot synthesis of pyrazolopyridines catalyzed by Fe_3O_4@SiO_2-SO_3H nanocatalyst under microwave irradiation. Sci Iran D Comput Sci Eng Electr Eng. 2017;24(3):1209–1219. https://doi.org/10.24200/SCI.2017.4105.
25. Zeynab S, Yagoub M. Fe_3O_4@SiO_2–SO_3H Nanoparticles: An efficient magnetically retrievable catalyst for esterification reactions. J Part Sci Technol.2018;4:67–79. https://doi.org/10.22104/jpst.2018.2811.1117.
26. Abdolkarim Z, Nesa L, Manije D. Preparation, characterization and application of nano-[Fe_3O_4@-SiO_2@ R-$NHMe_2$][H_2PO_4] as a novel magnetically recoverable catalyst for the synthesis of pyrimido [4,5-b] quinolines. J Mol Struct. 2020 July;1211:128030. https://doi.org/10.1016/j.molstruc.2020.128030.
27. Abbas N, Mushtaq A. Identification of active structure and catalytic efficiency of MCM-22 zeolite de templated by two different processes. J Porous Mater. 2021May;28:1439–1448. https://doi.org/10.1007/s10934-021-01098-w.
28. Md LR, Mohd S S, Mohammed SA, John J H, Shaheen MS, Silica-coated magnetic palladium nanocatalyst for Suzuki-Miyaura cross-coupling. Arabian J Chem. 2022;15(8):103983. https://doi.org/10.1016/j.arabjc.2022.103983.
29. Mohammad T. Athra GS, Kasim M H. Solid sulfamic acid catalyst for glucose production. J Phys: Con Ser. 2019;1294(5):052006. https://doi.org/10.1088/1742-6596/1294/5/052006
30. Sura HK, Hayder DA, Mohamed B, Mohamed L. Substituted Schiff bases for mild steel protection: corrosion inhibition performance, antibacterial activity, and quantum chemical

analysis. Chemistry Select.2025;10(45):e04378. https://doi.org/10.1002/slct.202504378
31. Athra GS, Jawad KA, Zeena R K. Molecular Docking, Synthesis and Evaluation for Antioxidant and Antibacterial Activity of New Oxazepane and Benzoxazepine Derivatives. Baghdad Sci J. 2024;21(7):2289. https://dx.doi.org/10.21123/bsj.2023.8553
32. Jain VS, Vora DK, Ramaa CS. Thiazolidine-2,4-diones: progress towards multifarious applications. Bioorg Med Chem.2013 Apr 1;21(7):1599–620. https://doi.org/10.1016/j.bmc.2013.01.029.
33. Ali SS, Kholoud DK, Jawad KA, Athra GS. Eco-assisted ultrasonic synthesis, characterization, and electrical conductivity study of polyaniline/silica@Fe_3O_4 Q1 nanocomposites, Karbala Int J Mod Sci. 2026;12(2) 234–242. https://doi.org/10.33640/2405-609X.3456
34. Mustafa A, Abbas N, Asim B. Montmorillonite clay modified by $CuFe_2O_4$ nanoparticles, an efficient heterogeneous catalyst for the solvent free microwave assisted synthesis of 1,3 thiazolidin 4 ones. Res Chem Int. 2024 Feb;50:1541–1556. https://doi.org/10.1007/s11164-024-05231-7.
35. Rajkumar R H, Praveen V S, Bhaskar R S, Murlidhar SS. Pd nanoparticles: an efficient catalyst for the solvent-free synthesis of 2,3-disubstituted-4-thiazolidinones. Res Chem Intermed. 2016;42:6695–6703. https://doi.org/10.1007/s11164-016-2490-2.
36. Manoj P T, Puneet K, Naresh K, Sushil K P. Silica gel promoted environment-friendly synthesis of 2,3-disubstituted 4-thiazolidinones. Tetrahedron Lett. 2014;55(15):2463–2466. https://doi.org/10.1016/j.tetlet.2014.03.007.
37. Naser F, Sattar E. One-pot synthesis of 1,3-thiazolidin-4-one using $Bi(SCH_2COOH)_3$ as catalyst. Chinese Chem Lett. 2013;24(5):389–391. https://doi.org/10.1016/j.cclet.2013.03.019.
38. Nagaraj B, Kanchan M, Raju ST, Kaliappan K, Yong RL. Sonochemical green Synthesis of yttrium Oxide(Y_2O_3)nanoparticles as a novel heterogeneous catalyst for the construction of biologically interesting 1,3-thiazolidin-4-ones. Catal Lett.2017;147: 2630–2639. https://doi.org/10.1007/s10562-017-2168-4.
39. Ganapavarapu VRS, Bandaru D, Karri SR, Mallidi V R, Anand K K, Cherukuvada B. Montmorillonite K10 catalyzed multi component reactions (MCR):synthesis of novel thiazolidinones as anticancer agents. Heterocycl Commun. 2015;21(4):187–190. https://doi.org/10.1515/hc-2015-0035.
40. Mohammad N, Leila ZF, Fariba S, Hasti T. Green synthesis of pyrazolo-thiazolidine-4-ones using magnetic nanocomposite of multiwalled carbon nanotube. J Heterocycl Chem. 2018;55(8):1973–1977. https://doi.org/10.1002/jhet.3237.
41. Mehdi K, Soodabeh B, Seyed A M. Ni@zeolite-Y nanoporous;a valuable and efficient nanocatalyst for the synthesis of N-benzimidazole-1,3-thiazolidinones. Green Chem Lett Rev.2018;11(3):334–344. https://doi.org/10.1080/17518253.2018.1499968.
42. Mojtaba L, Majid G. Preparation of thiazolidin-4-one derivatives using ZnO–NiO–$NiFe_2O_4$ nano-composite system. Res Chem Intermed. 2021;47(2):589–597. https://doi.org/10.1007/s11164-020-04287-5.
43. Mohammad N, Leila Z F, Hasti T. Green synthesis of novel 2-pyrazolyl-1,3-thiazolidine-4-ones using 2-oxoimidazolidine-1,3-disulfonic acid. Heterocycl Commun. 2017;23(6):429–432. https://doi.org/10.1515/hc-2017-0124

تحضير وتشخيص مركبات 1،3-ثيازوليدين-4-أون باستخدام حفاز نانوي مغناطيسي، قابل لإعادة التدوير، في وسط اشعة ميكروويف وخالٍ من المذيبات

جواد كاظم عبيس، عذراء كطامي صكر، زينه رزاق كطوف

قسم الكيمياء، كلية العلوم، جامعة واسط، واسط، العراق.

الخلاصة

في هذا العمل، استُخدم محفز نانوي صديق للبيئة (γ Fe2O3RHA@SO3H) لتحضير مشتقات 1،3-ثيازوليدين-4-أونز (T1-T9) من قواعد شيف (S1-S9) بواسطة إشعاع الميكروويف. أُنتج المحفز المعاد تدويره (γ Fe2O3RHA@SO3H) من السيليكا المشتقة من قشر الأرز، والتي عُدِّلت أولًا بجسيمات نانوية من اوكسيد الحديد (Fe2O3)، ثم بحامض الكبريتيك. تم تشخيص الخصائص النانويه للمركب (γFe2O3RHA@SO3H)، بما في ذلك صوره السطح، باستخدام حيود الأشعة السينية(XRD)، والحموضة الكلية والقاعدية باستخدام CO2/NH3-TPD، والخصائص النسيجية من خلال بروناور-إيميت-تيلر (BET)، وتحديد المجموعة الوظيفية بواسطة FTIR؛ تم فحص مورفولوجيا السطح باستخدام مجهر FE-SEM ومجهر TEM، والخصائص المغناطيسية باستخدام مقياس مغناطيسية العينة المهتزة (VSM)، والاستقرار الحراري باستخدام التحليل الحراري الوزني (TGA). أظهرت بيانات مقياس مغناطيسية العينة المهتزة (VSM) إمكانية فصل المحفز فائق المغناطيسية (γ Fe2O3RHA@SO3H) واستعادته بسهولة بعد اكتمال التفاعل باستخدام مغنطة خارجية. وكشفت البيانات أن ظروف التفاعل المثلى للمحفز (γ Fe2O3RHA@SO3H) لإنتاج (S1-S9) كانت 5% من المحفز، والإيثانول كمذيب، ووقت تفاعل ساعة واحدة، ودرجة حرارة تفاعل 70 درجة مئوية، مع أقصى إنتاجية تصل إلى 94%. وأظهرت نتائج دراسة إمكانية إعادة الاستخدام وإعادة التنشيط أن المحفز المغناطيسي النانوي ثنائي الوظيفة (γ Fe2O3RHA@SO3H) يمكنه الحفاظ على نشاط تحفيزي عالٍ بعد إعادة استخدامه ثلاث مرات على الأقل. وأشارت النتائج أيضًا إلى أن المحفز(γ Fe2O3RHA@SO3H) يتمتع بخصائص مغناطيسية جيده مما يجعل امكانيه استخدامه كمحفز غير متجانس في إنشاء مشتقات 1،3-ثيازوليدين-4-ون بكفاءة عالية في ظروف التفاعل البسيطة.

الكلمات المفتاحية: المحفز، الجسيمات النانوية، إعادة التدوير، قاعدة شيف، سليكا.